

# 1 Quantifying immediate carbon emissions from El Niño-mediated wildfires in 2 humid tropical forests

3 Kieran Withey\*<sup>1</sup>, Erika Berenguer<sup>1,2</sup>, Alessandro Ferraz Palmeira<sup>3</sup>, Fernando D. B. Espírito-  
4 Santo<sup>4</sup>, Gareth D. Lennox<sup>1</sup>, Camila V. J. Silva<sup>1</sup>, Luiz E. O. C. Aragão<sup>5,6</sup>, Joice Ferreira<sup>7</sup>, Filipe  
5 França<sup>1,7,8</sup>, Yadvinder Malhi<sup>2</sup>, Liana Chesini Rossi<sup>9</sup>, Jos Barlow<sup>1</sup>

6 <sup>1</sup>Lancaster Environment Centre, Lancaster University, Lancaster, LA1 4YQ, UK.

7 <sup>2</sup>Environmental Change Institute, University of Oxford, Oxford, OX1 3QY, UK.

8 <sup>3</sup>Instituto de Ciências Biológicas, Universidade Federal do Pará, Rua Augusto  
9 Corrêa, 01, Campus Guamá, Belém, PA, Brazil - CEP: 66075-110.

10 <sup>4</sup>Centre for Landscape and Climate Research (CLCR) and Leicester Institute of  
11 Space and Earth Observation (LISEO), School of Geography, Geology and  
12 Environment, University of Leicester, University Road, Leicester, LE1 7RH.

13 <sup>5</sup>Remote Sensing Division, National Institute for Space Research, Av. dos  
14 Astronautas, 1.758, 12227-010 São José dos Campos, SP, Brazil.

15 <sup>6</sup>College of Life and Environmental Sciences, University of Exeter, Exeter EX4 4RJ,  
16 UK.

17 <sup>7</sup>Embrapa Amazônia Oriental, Trav. Dr. Enéas Pinheiro, s/n, CP 48, 66095-100,  
18 Belém, PA, Brazil.

19 <sup>8</sup>Instituto Federal de Minas Gerais, Rodovia Bambuí/Medeiros, Km-05, 38900-000,  
20 Bambuí, MG, Brazil.

21 <sup>9</sup>Departamento de Ecologia, Universidade Estadual Paulista, 13506-900, Rio Claro,  
22 SP, Brazil.

23 Keywords: (1) ENSO; (2) forest degradation; (3) climate change; (4) necromass; (5)  
24 drought; (6) Amazon

25 \*Author for correspondence (kieranwithey@gmail.com).

## 26 Summary

27 Wildfires produce substantial CO<sub>2</sub> emissions in the humid tropics during El Niño-mediated  
28 extreme droughts, and these emissions are expected to increase in coming decades. Immediate  
29 carbon emissions from uncontrolled wildfires in human-modified tropical forests can be  
30 considerable due to high necromass fuel loads. Yet, data on necromass combustion during  
31 wildfires is severely lacking. Here, we evaluated necromass carbon stocks before and after the  
32 2015-16 El Niño in Amazonian forests along a gradient of prior human disturbance. We then  
33 used Landsat-derived burn scars to extrapolate regional immediate wildfire CO<sub>2</sub> emissions  
34 during the 2015-16 El Niño. Before the El Niño, necromass stocks varied significantly with  
35 respect to prior disturbance and were largest in undisturbed primary forests (30.2 ± 2.1 Mg ha<sup>-1</sup>,  
36 mean ± se) and smallest in secondary forests (15.6 ± 3.0 Mg ha<sup>-1</sup>). However, neither prior  
37 disturbance nor our proxy of fire intensity (median char height) explained necromass losses due  
38 to wildfires. In our 6.5 million ha study region, almost 1 million ha of primary (disturbed and  
39 undisturbed) and 20,000 ha of secondary forest burned during the 2015-16 El Niño. Covering  
40 <0.2% of Brazilian Amazonia, these wildfires resulted in expected immediate CO<sub>2</sub> emissions of

41 approximately 30 Tg, 3-4 times greater than comparable estimates from global fire emissions  
42 databases. Uncontrolled understorey wildfires in humid tropical forests during extreme droughts  
43 are a large and poorly quantified source of CO<sub>2</sub> emissions.

## 44 1. Introduction

45 Increased concentrations of atmospheric CO<sub>2</sub> during El Niño Southern Oscillation events [1,2]  
46 have largely been attributed to emissions from the tropics [3,4], with wildfires playing an  
47 important role [4,5]. In recent decades, despite a global reduction in burned vegetation area  
48 [6,7], relatively low-intensity understorey wildfires that spread from agricultural lands have  
49 increased in the fire-sensitive Amazon rainforest [8–11]. CO<sub>2</sub> emissions from such wildfires are  
50 expected to grow further [10] as fire-conducive weather patterns increase across the humid  
51 tropics, particularly in South America [12].

52 Large-scale understorey wildfires in Amazonia are unprecedented in recent millennia. During  
53 pre-Columbian times, fires were limited to those occurring naturally from lightning strikes and  
54 prescribed burns by indigenous peoples [13]. These fires were localised and prescribed burns  
55 were planned in accordance with environmental and ecological conditions [13]. However,  
56 pervasive human modification of tropical forest landscapes, through, for example, road building,  
57 cattle ranching, and timber exploitation, combined with unprecedented drought events and the  
58 widespread use of fire as a land management tool, has fundamentally altered Amazonian fire  
59 regimes. Today, uncontrolled large-scale understorey wildfires are being witnessed in the  
60 Amazon with sub-decadal frequency [14]. Such wildfires result in high rates of tree mortality  
61 [15,16], shifts in forest structure [17,18], and drier microclimatic conditions [19], ultimately  
62 leading to increased susceptibility to future wildfires [19–21].

63 Carbon emissions from understorey wildfires can be split into committed and immediate  
64 emissions. Committed emissions result from the complex interplay between delayed tree  
65 mortality and decomposition, and are dependent on future climatic conditions and human  
66 influences. Research indicates that long-term storage of carbon in wildfire-affected Amazonian  
67 forests can be compromised for at least several decades: even 31 years after a fire event,  
68 burned forests store ~25% less carbon than unburned control sites due to high levels of tree  
69 mortality that are not compensated by regrowth [22]. Immediate understorey emissions are  
70 those that occur during wildfires and, in contrast to committed emissions, are relatively simple to  
71 estimate. Biome- and continent-wide analyses that rely on satellite observations (known as top-  
72 down studies) suggest that these immediate emissions from tropical forests can be substantial  
73 [23,24] and, for example, can transform the Amazon basin from a carbon sink to a large carbon  
74 source during drought years [25].

75 One potentially important source of immediate carbon emissions during wildfires is dead organic  
76 matter found on forest floors. This necromass, which includes leaf litter and woody debris, is a  
77 fundamental component of forest structure and dynamics and can account for up to 40% of the  
78 carbon stored in humid tropical forests [26–28]. During long periods of drought, this large carbon  
79 pool can become highly flammable [29]. However, studies quantifying necromass stocks have  
80 overwhelmingly focused on undisturbed primary forests [27]; studies that estimate necromass in  
81 human-modified tropical forests – forests that have been structurally altered by anthropogenic

82 disturbance, such as selective logging and fires, and those regenerating following deforestation  
83 (commonly called *secondary forests*; table 1) – are rare (c.f. [30,31]). This represents a key gap  
84 in our understanding because human-modified tropical forests are increasingly prevalent [32]  
85 and increasingly vulnerable to wildfires [33-35]. While many local-scale, bottom-up studies have  
86 quantified combustion characteristics and carbon emissions following fires related to  
87 deforestation and slash-and-burn practices (see Leeuwen et al. [36] for a recent review), we  
88 know of no study that quantifies necromass before and after uncontrolled understorey wildfires  
89 in human-modified Amazonian forests. These knowledge gaps and data shortfalls limit our  
90 understanding of immediate carbon emissions from understorey wildfires. Improving such  
91 estimates is essential for refining Earth Systems models and both national and global estimates  
92 of greenhouse gas emissions.

93 Here, we address these knowledge gaps using a hybrid bottom-up/top-down approach to study  
94 a human-modified region of central-eastern Amazonia which experienced almost 1 million ha of  
95 understorey wildfires during the 2015-16 El Niño (figure 1). We combined data from a previously  
96 published large-scale field assessment of carbon stocks [37] with on-the-ground measures of  
97 woody debris before and after the 2015-16 El Niño, proxies of fire intensity and coverage within  
98 study plots, and remotely sensed analyses of fire extent across the region. Specifically, we (a)  
99 quantify carbon stocks vulnerable to combustion across human-modified tropical forests in  
100 central-eastern Amazonia; (b) use post-burn measures to investigate the factors influencing the  
101 loss of necromass during wildfires; (c) estimate region-wide immediate carbon emissions from  
102 wildfires; and (d) compare these region-wide emission estimates to those derived from widely  
103 used global fire emissions databases.

## 104 2. Methods

### 105 (a) Quantification of necromass stocks in human-modified Amazonian forests

106 We established 107 plots (0.25 ha) in human-modified forests in central-eastern Amazonia in  
107 2010 (figure 1). Plots were located in the municipalities of Santarém, Belterra, and Mojuí dos  
108 Campos in the state of Pará, Brazil, and form part of the Sustainable Amazon Network (RAS –  
109 *Rede Amazônia Sustentável* in Portuguese [38]). Study plots covered a range of prior human  
110 impacts (table 1) and included undisturbed primary forests ( $n = 17$ ), primary forests selectively  
111 logged prior to 2010 ( $n = 26$ ), primary forests burned prior to 2010 ( $n = 7$ ), primary forests  
112 logged and burned prior to 2010 ( $n = 24$ ), and secondary forests recovering after complete  
113 removal of vegetation ( $n = 33$ ; see table 1).

114 Summary carbon estimates for these 107 plots can be found in Berenguer et al. [37]. Here, we  
115 focused on carbon stored in their necromass pools. We estimated necromass stocks in dead-  
116 standing tree and palm stems, coarse woody debris (CWD;  $\geq 10$  cm diameter at one extremity),  
117 fine woody debris (FWD; 2-10 cm diameter at both extremities), and leaf litter (including twigs  $<$   
118 2 cm diameter at both extremities, leaves, and fruits and seeds). Full carbon estimation methods  
119 can be found in Berenguer et al. [37]. In brief, in each plot we measured the diameter and height  
120 of all large ( $\geq 10$ cm DBH) dead tree and palm stems. We measured the diameter and height of  
121 all small dead tree and palm stems ( $\geq 2$ -10 DBH) in five subplots (5 x 20 m) in each plot. We  
122 used the allometric equations of Hughes et al. [39] and Cummings et al. [40] to estimate,

123 respectively, carbon stocks for dead-standing trees and palms. Subplots were also used to  
124 estimate the diameters and lengths of all pieces of fallen CWD ( $\geq 10$  cm). We estimated the  
125 volume of each piece of CWD using Smalian's formula [27] after accounting for the extent of  
126 damage (i.e. void space). We multiplied the volume of each CWD piece by its decomposition  
127 class to calculate CWD mass [41]. In all study plots, we established five smaller subplots (2 x 5  
128 m) to assess fine woody debris (FWD). These were sampled and weighed in the field. A sub-  
129 sample ( $\leq 1$  kg) was collected in each subplot and oven-dried to a constant weight. The wet-to-  
130 dry ratios of the FWD samples were used to estimate the total FWD stocks per plot. To estimate  
131 the biomass of leaf litter, ten 0.5 x 0.5 m quadrats were established in each plot. We oven-dried  
132 leaf litter samples to a constant weight to get an estimate of the leaf litter stocks in each plot.  
133 Biomass estimates for each necromass component were then standardised to per ha values,  
134 and the carbon content was assumed to be 50% of biomass dry weight [42]. See  
135 Supplementary Materials (Section 1) for all equations we used to estimate necromass biomass.

### 136 (b) Longitudinal monitoring of coarse woody debris

137 To estimate necromass change through time, we continued to monitor 18 of the 107 RAS plots  
138 (figure 1). These 18 plots were chosen because they are spatially distributed across the region  
139 and we were able to secure long-term authorization to monitor them. They included undisturbed  
140 primary forests ( $n = 5$ ), primary forests logged prior to 2010 ( $n = 5$ ), primary forest logged and  
141 burned prior to 2010 ( $n = 4$ ), and secondary forests ( $n = 4$ ; table 1). We conducted surveys of  
142 the 18 plots between November 2014 and September 2015, using a slightly altered sampling  
143 design to align with the Global Ecosystem Monitoring (GEM) protocol (see [43] for details). We  
144 established five 1 x 20 m subplots in each of the 18 plots, measured all pieces of CWD, and  
145 estimated their biomass and carbon content following the methods outlined above (see Methods  
146 (a)).

### 147 (c) Impacts of El Niño mediated wildfires on necromass stocks

148 Extensive understorey wildfires burned seven of our 18 study plots during the 2015-16 El Niño,  
149 including two previously undisturbed primary forests, four primary forests logged prior to 2010,  
150 and one primary forest that was logged and burned prior to 2010. To investigate necromass  
151 carbon stock losses due to these wildfires, we resurveyed all 18 plots in June 2017. We re-  
152 measured each individual piece of CWD and estimated biomass using the methods described  
153 above (Methods (a)). By comparing CWD stocks before and after the El Niño in the 11 plots that  
154 did not experience wildfires, we were able to estimate CWD background decomposition rates.  
155 By comparing CWD stocks before and after the El Niño in the seven plots that did suffer  
156 wildfires, we were able to measure CWD combustion completeness.

157 We used values from the 2010 surveys to provide estimates of the pre-El Niño carbon stocks in  
158 leaf litter and FWD. Based on visual inspection of the sites (figure S2), we assumed 100%  
159 combustion completeness of these necromass components in the fire-affected proportion of  
160 burned plots. Recognising that this is a strong assumption, we consider the validity of it in our  
161 Discussion. We did not consider wildfire-mediated changes in necromass carbon stocks in dead  
162 standing trees and palms, due to a lack of data on combustion completeness.

163 In the seven plots that burned, we calculated average char height for each stem, defined as the  
164 sum of maximum and minimum char heights divided by two. We then used these average stem  
165 char heights to calculate the plot-level median char height, which we used as our proxy for fire  
166 intensity. In addition, we used the proportion of sampled stems with burn scars as an estimate of  
167 the area of each plot that burned (Supplementary Materials). To increase our sample of fire-  
168 affected plots (to 16), we also measured the area burned in an additional 9 of the original RAS  
169 plots that were sampled during the 2010 censuses and burned during 2015-16 (table 1). Prior to  
170 the wildfires, these additional plots included undisturbed primary forests ( $n = 3$ ), primary forests  
171 logged prior to 2010 ( $n = 1$ ), primary forests logged and burned prior to 2010 ( $n = 4$ ), and  
172 secondary forests ( $n = 1$ ).

173 We used these data to estimate the per ha necromass loss (NL) attributable to wildfires using  
174 the following equation:

$$175 \quad NL = FL_{CWD} \times (CC_{CWD} - D_{CWD}) + FL_{LLFWD} \times BA \quad (1)$$

176 where,  $FL_{CWD}$  is the per ha fuel load of CWD estimated from the 107 RAS plots surveyed in  
177 2010;  $CC_{CWD}$  is the combustion completeness of CWD estimated from seven of the 18 CWD  
178 monitoring plots that burned during the 2015-16 El Niño;  $D_{CWD}$  is the background CWD  
179 decomposition rate estimated from the 11 CWD monitoring plots that did not burn during the  
180 2015-16 El Niño;  $FL_{LLFWD}$  is the per ha fuel load of leaf litter and FWD estimated from the 107  
181 plots surveyed in 2010; and BA the proportion of the plot that burned estimated from the 16 RAS  
182 plots that burned during the 2015-16 El Niño (table 1).

#### 183 (d) Data analysis

184 We used the Kruskal-Wallis test to investigate variation across forest classes of prior human  
185 disturbance (table 1) and used the Conover-Iman test with Bonferroni adjustments to perform  
186 multiple pairwise comparisons of forest class medians. We assessed differences across forest  
187 classes in: carbon stocks stored in each necromass component (i.e., dead-standing stems,  
188 CWD, FWD, and leaf litter) from the 2010 survey; total and percentage necromass carbon stock  
189 losses in the 18 plots surveyed between 2014 and 2017; and the proportion / area of plots  
190 burned during the 2015-16 El Niño. We used linear regression to investigate the relationship  
191 between: necromass carbon stocks before and after the 2015-16 El Niño; fire intensity and stock  
192 losses; and the burned area in each plot and stock losses.

193

#### 194 (e) Quantification of burned area and estimation of region-wide emissions from forest fires

195 To estimate wildfire-mediated carbon emissions from necromass across our study region, we  
196 first calculated the cumulative area of primary and secondary forest that experienced  
197 understory wildfires during 2015-16 in the central-eastern region of the Amazon, an area of  
198 ~6.5 million ha (figure 1). We built a time-series of Landsat (5, 7 and 8) imagery from 2010 to  
199 2017 for the RAS study region and the surrounding area from the EROS Science Processing  
200 Architecture (ESPA) / U.S. Geological Survey (USGS) website (<https://espa.cr.usgs.gov>). We  
201 performed an unsupervised classification of raw imagery, followed by manual correction of

202 classification errors, to identify several land-uses throughout the time-series (see table S2 for all  
203 land-use classes and the Supplementary Materials Section 2 for a detailed description of burned  
204 areas detection). We then used the burned area of primary and secondary forests and estimates  
205 of per ha necromass stock losses from wildfires (Eq. 1) to determine region-wide necromass  
206 carbon emissions, using a conversion factor of 3.286 kg of CO<sub>2</sub> per kg of C [44]. This conversion  
207 factor does not include other forms of emitted C (such as CO), in keeping with global fire  
208 emissions databases.

209 We took two approaches to account for uncertainty in expected regional necromass emissions.  
210 First, we considered four land-use scenarios using two sets of primary and secondary forests  
211 (table S1). To account for potential variation in fire susceptibility across primary forest  
212 disturbance classes, we estimated the five variables in Eq. 1 using all undisturbed and disturbed  
213 primary forest classes (prim1) and then only disturbed primary forests (prim2). For secondary  
214 forests, we used CC<sub>CWD</sub> and FL<sub>LLFWD</sub> from all secondary forests, used D<sub>CWD</sub> and BA from all  
215 forest classes combined, and used CC<sub>CWD</sub> from all primary forest classes because none of the  
216 secondary forests plots we were monitoring for changes in CWD burned during 2015-16 (sec1).  
217 Our other scenario for secondary forests (sec2) was more restrictive: we used the fuel load (FL<sub>CWD</sub>,  
218 FL<sub>LLFWD</sub>), decomposition (D<sub>CWD</sub>), and BA values from secondary forests only and combined  
219 these with all CC<sub>CWD</sub> values we had from disturbed and undisturbed primary forests.

220 Second, to account for uncertainty in the distribution of the variables in Eq. 1, we ran 1000  
221 bootstrap with replacement simulations to determine each variable's mean value and standard  
222 error. We calculated the standard error of Eq. 1 using the variable standard errors, accounting  
223 for error propagation, and we constructed 95% confidence intervals for Eq. 1 as its mean value  
224 ± 1.96 times the standard error of the mean.

#### 225 (f) Quantitative comparisons with GFED and GFAS

226 We compared our region-wide CO<sub>2</sub> emission estimates to two fire emissions databases  
227 frequently used in Earth Systems models and carbon budgets: the Global Fire Emissions  
228 Database (GFED) version 4.1s [45] and the Global Fire Assimilation System (GFAS) version 1.1  
229 [46]. For both datasets, we obtained data for our study period (August 2015 – July 2016) and  
230 cropped them to our ~6.5 million ha study region, shown in figure 1.

231 We first calculated cumulative emissions from GFED and GFAS (Supplementary Materials) and  
232 compared these to our emissions estimates. Second, to investigate potential sources of  
233 discrepancy between estimates, we spatially mapped GFED, GFAS, and our CO<sub>2</sub> emissions  
234 estimates. At both GFED and GFAS resolutions (0.25 and 0.1 degrees, respectively), we  
235 mapped our mean (across land-use scenarios; table S1) expected emissions assuming that  
236 emissions were constant in burned area (i.e. if a cell contained x% of the burned area, we  
237 assumed it accounted x% of the total emissions). Finally, because GFED also provides  
238 estimates of the area burned at 0.25 degrees, we used our land-use map to estimate burned  
239 area at that resolution.

### 240 3. Results

### 241 (a) Vulnerable necromass carbon stocks across human-modified Amazonian forests

242 Total necromass and its components varied significantly with respect to forest class ( $p < 0.05$  in  
243 all cases; figure 2). Primary forests contained significantly higher total necromass than  
244 secondary forests ( $p < 0.01$  for all pairwise comparisons), with the highest total found in  
245 undisturbed primary forests ( $30.2 \pm 2.1 \text{ Mg ha}^{-1}$ , mean  $\pm$  se). By contrast, secondary forests  
246 contained only half as much necromass as undisturbed primary forests ( $15.6 \pm 3.0 \text{ Mg ha}^{-1}$ ).  
247 Variation in total necromass was driven in large part by variation in CWD, which accounted for  
248  $61.3 \pm 2.7\%$  of the total necromass stocks across forest classes. Leaf litter was the next most  
249 important component of total necromass, with  $19.8 \pm 2.7\%$  residing in this component. Dead  
250 standing stems accounted for  $14.4 \pm 1.8\%$  of total necromass. Finally, FWD was by far the  
251 smallest necromass component, harbouring just  $4.6 \pm 0.2\%$  of the total.

### 252 (b) Impacts of El Niño mediated wildfires on necromass stocks

253 On average,  $87.1 \pm 2.7\%$  of the ground area of our fire-affected study plots burned, and there  
254 was no significant difference in the total unburned area of fire-affected plots across forest  
255 classes ( $\chi^2_3 = 2.1$ ;  $p = 0.56$ ). For CWD, all but two pieces had burned from a total of 34, and  
256 CWD carbon stocks losses from combustion varied from 38% to 94% (mean = 65.4%, SE =  
257 7.1%).

258 Necromass carbon stock losses in the seven burned plots were unrelated to median char height  
259 ( $R^2 = 0.09$ ;  $p = 0.51$ ; figure 3a) and area of plot burned ( $R^2 = 0.10$ ;  $p = 0.49$ ; figure 3b). Forest  
260 class did not predict necromass carbon stock losses in burned sites when expressed as either  
261 percentage ( $\chi^2_2 = 2.25$ ;  $p = 0.32$ ) or total ( $\chi^2_2 = 1.12$ ;  $p = 0.57$ ) loss. Similarly, forest class did not  
262 predict necromass losses in unburned sites when expressed as either percentage ( $\chi^2_3 = 1.58$ ;  $p$   
263 = 0.66) or total ( $\chi^2_3 = 2.18$ ;  $p = 0.54$ ) loss.

264 On average, burned sites lost  $73.0 \pm 4.9\%$  of their pre-El Niño necromass stocks (figure 4),  
265 compared to a  $26.1 \pm 4.8\%$  reduction in unburned sites (from decomposition). As expected, pre-  
266 El Niño necromass stocks strongly predicted post-El Niño necromass in our unburned sites ( $R^2$   
267 = 0.95;  $p < 0.001$ ; figure 4a). This relationship disappeared in fire-affected plots ( $R^2 = 0.08$ ;  $p$   
268 = 0.54; figure 4b), indicating that combustion completeness was insensitive to initial necromass  
269 stocks. Despite our small sample size, visual inspection suggests that these findings were  
270 unaffected by forest class.

### 271 (c) Region-wide burned area and estimates of carbon stock losses

272 During the 2015-16 El Niño, 982,276 ha (15.2%) of forest in our study region experienced  
273 understory wildfires. These wildfires were overwhelmingly concentrated in primary forests:  
274 <2% of the burned area was in secondary forests, despite these accounting for 9% of the forest  
275 cover in our study region. When considering all primary forest and secondary forest plots (prim1  
276 + sec1), resultant necromass carbon stock losses amounted to 10.06 Tg (95% confidence  
277 interval, 5.85-14.27 Tg). Converting to CO<sub>2</sub>, this is equivalent to expected emissions of 33.05 Tg

278 (95% confidence interval, 19.22-46.87 Tg; figure 5). Our mean carbon-dioxide emission  
279 estimates were relatively insensitive to the land-use scenarios (figure 5). However, the 95%  
280 confidence interval was substantially wider with land-use scenario prim2 (scenarios b & d; figure  
281 5) due to greater uncertainty in decomposition rates when restricted to disturbed primary forest  
282 only compared to all primary forests – undisturbed and undisturbed – combined.

#### 283 (d) CO<sub>2</sub> emissions comparison with GFED and GFAS

284 GFED and GFAS both vastly underestimated expected wildfire CO<sub>2</sub> emissions for our study  
285 region and period. Respectively, these databases suggest cumulative emissions that are 77%  
286 and 68% lower than the expected value we found with land-use scenario a (figure 5). These  
287 discrepancies can be explained by the underdetection of understory wildfires by both GFED  
288 and GFAS algorithms. This can be seen across our whole study region, but is particularly  
289 evident in areas free from historic deforestation (figure 6). GFED and GFAS appear to be more  
290 successful at detecting fires in agricultural areas with lower levels of forest cover (figure 6).  
291 Highlighting the insensitivity of GFED to understory wildfires, this database suggests that, at  
292 most, 6% of any given 0.25-degree cell across our study region, and approximately 90,000 ha in  
293 total, burned during the 2015-16 El-Niño (figure 6e). By contrast, we show that as much as 74%  
294 of a cell (figure 6f) and almost 1 million ha of forest was affected by understory wildfires.

## 295 4. Discussion

### 296 (a) Region-wide carbon emissions from El Niño-mediated wildfires

297 We investigated necromass carbon stocks in human-modified forests before and after large-  
298 scale understory wildfires in central-eastern Amazonia that occurred during the 2015-16 El  
299 Niño. Our novel assessment revealed that expected immediate necromass CO<sub>2</sub> emissions from  
300 these wildfires are around 30 Tg (figure 5). This is equivalent to total CO<sub>2</sub> emissions from fossil  
301 fuel combustion and the production of cement in Denmark, or 6% of such emissions from Brazil,  
302 in 2014 [47]. Consequently, wildfire-mediated immediate carbon emissions, which are not  
303 currently considered under national greenhouse gas inventories [48], represent a large source  
304 of CO<sub>2</sub> emissions. Moreover, these immediate emissions will be greatly exacerbated by further  
305 committed emissions resulting from tree mortality, which can be as high as 50% [16] and may  
306 not be balanced by post-fire regrowth on decadal time scales [22].

307 Our results add to the work on prescribed burns associated with deforestation [36], contributing  
308 important information about the role of El Niño-mediated wildfires. The scale of the immediate  
309 emissions we estimated, coupled with future committed emissions, make wildfires particularly  
310 relevant for climate change mitigation programmes such as REDD+ [9,49]. For REDD+ to  
311 succeed in Amazonia, we demonstrate that forests must be protected from wildfires, as even the  
312 immediate emissions from large-scale wildfires can equal those from whole countries. Future  
313 climate change will make this only more imperative, with extreme droughts, higher  
314 temperatures, and reduced rainfall all predicted for the Amazon Basin in the near future [50–52].  
315 Wildfires may also undermine the important role that protected areas have historically served as  
316 carbon stores [53], as illustrated by the large areas burned in the Tapajós National Forest and  
317 the Tapajós-Arapiuns Extractive Reserve (figure 1).

## 318 (b) Fuel loads in humid tropical forests

319 Total necromass carbon stocks in the 107 RAS plots surveyed in 2010 did not vary significantly  
320 between disturbed and undisturbed primary forests (figure 2e). The mean value we found for  
321 total necromass carbon stocks in undisturbed forests was  $30.2 \pm 2.1 \text{ Mg ha}^{-1}$ . This value is  
322 broadly consistent with previous estimates for the eastern Amazon. For example, Keller et al.  
323 [41] and Palace et al. [54] found necromass carbon stocks of, respectively, 25.4 and 29.2 Mg  
324  $\text{ha}^{-1}$  in undisturbed primary forests in the Tapajós region of Pará. In primary forests disturbed by  
325 reduced-impact logging, these studies found, respectively, 36.4 and 42.75  $\text{Mg ha}^{-1}$  of  
326 necromass carbon. However, our estimates for necromass stocks in disturbed primary forests  
327 are markedly lower (figure 2e). This discrepancy is likely a function of time since disturbance.  
328 Keller et al. [41] and Palace et al. [54] assessed necromass carbon stocks soon after  
329 disturbance, when necromass stocks are likely to be higher. In contrast, disturbance of RAS  
330 sites occurred between 1.5 and 25 years before the 2010 surveys. Necromass stocks can be  
331 highly dynamic, with residence times for most coarse woody debris estimated at less than a  
332 decade [28], especially in the case of small diameter and low wood density tree species [55].  
333 Thus, necromass stocks in many of our disturbed primary forest sites may have had time to  
334 decrease to an equilibrium level, similar to that of undisturbed forests, where input and  
335 decomposition are largely balanced.

336 We did, however, find significantly larger necromass stocks in primary forests compared to  
337 secondary forests. This may be explained by a) pre-abandonment land-uses removing all fallen  
338 biomass in intensive clearance or maintenance fires; b) the smaller necromass input pool in  
339 secondary forests due to lower levels of aboveground live biomass [37]; and c) the lower wood  
340 density of stems in secondary forests [56], resulting in more rapid coarse woody debris  
341 decomposition.

## 342 (c) Impacts of El Niño mediated wildfires on necromass stocks

343 On average, wildfires burned  $87.1 \pm 2.7\%$  of our fire-affected necromass monitoring plots (figure  
344 3b). This figure is substantially higher than the 62-75% burn coverage measured during  
345 experimental fires in previously undisturbed transitional Amazonian forests [18]. The areal  
346 extent of these wildfires reduced necromass (in CWD, FWD, and leaf litter) carbon stocks by  
347  $46.9 \pm 6.9\%$ , when gross necromass loss ( $73.0 \pm 4.9\%$ ) was corrected for decomposition ( $26.1 \pm$   
348  $4.8\%$ ). The understory wildfires that affected our burned plots were relatively low intensity, with  
349 maximum median char height of 20.5 cm. Nonetheless, our findings demonstrate that these low-  
350 intensity wildfires can dramatically diminish necromass stocks in human-modified tropical  
351 forests.

352 Further, both area of plot burned and necromass carbon stock losses showed little variation  
353 across disturbance classes. This may indicate that the 2015-16 El Niño, which was one of the  
354 strongest in recorded history, produced drought conditions so severe that necromass moisture  
355 content was reduced across all forest classes to a level which permitted combustion and  
356 sustained fires, overriding any pre-existing microclimatic differences that may have existed due  
357 to the initial disturbance. This is further corroborated by the fact that wildfires did not distinguish  
358 between largely undisturbed forests (mostly inside protected areas) and those that have been

359 modified by humans (mostly outside protected areas), burning vast areas of both types of forest  
360 (figure 1).

#### 361 (d) Caveats

362 Though our dataset is the first that allows for quantification of necromass carbon stocks pre- and  
363 post-uncontrolled understory wildfires in human-modified Amazonian forests, our sample size  
364 was limited, with just 18 necromass monitoring plots, of which seven burned during the 2015-16  
365 El Niño. Consequently, results which follow from these samples should be treated with a degree  
366 of caution. In particular, we found that necromass stock losses were not significantly related to  
367 our plot-level estimate of burned area and that fire susceptibility did not appear to vary across  
368 disturbance classes. In both cases, the lack of significance may reflect the small sample sizes  
369 rather than a genuine lack of relationship.

370 Moreover, due to the limitations of our data, we assumed 100% combustion of leaf litter and  
371 FWD in the fraction of plots that burned when calculating necromass carbon losses (Eq. 1). In a  
372 recent review, Leeuwen et al. [36] found that mean combustion completeness of leaves, litter,  
373 and smaller classes of woody debris was 73-94%. However, as they acknowledge, combustion  
374 completeness can be significantly higher during El Niño years. Thus, given the strength of the  
375 2015-16 El Niño, and our personal observations (figure S2), our combustion completeness  
376 assumption is likely to be reasonable.

377 Because of our small sample size, the 95% confidence intervals for our region-wide CO<sub>2</sub>  
378 immediate emissions are wide, ranging from around 8 Tg to almost 48 Tg. Future research  
379 efforts should prioritise necromass monitoring in a larger number of sites, across a range of  
380 tropical forests, to better constrain these values; as we show, such emissions have the potential  
381 to significantly exacerbate global climate change.

382 Despite the above limitations, there are reasons to suspect that our necromass stock loss and  
383 carbon emission estimates are highly conservative. First, we did not measure wildfire-induced  
384 carbon changes in the soil organic layer, yet research from the same region suggests that  
385 wildfires significantly reduce soil carbon pools [57]; nor could we estimate combustion of dead-  
386 standing stems, which account for ~15% of total necromass (figure 2). Second, none of the  
387 disturbed primary forest plots in which we monitored necromass changes were recently  
388 disturbed prior to the 2015-16 wildfires, allowing time for decomposition to reduce high levels of  
389 post-disturbance necromass. Had our sample included recently disturbed sites, necromass  
390 losses would have been greater. Third, detection of low intensity understory wildfires continues  
391 to present a remote sensing challenge. Although manual correction of our unsupervised land-  
392 use classifications revealed only a small number of misclassifications, it is possible that some  
393 wildfire-affected sites were missed, leading to an underestimation of regional emissions.

394 In addition to showing that wildfire carbon emissions can be substantial, we also showed that  
395 such emissions remain poorly quantified. GFED and GFAS, CO<sub>2</sub> emission databases that are  
396 widely used in Earth Systems models and carbon budgets, returned considerably lower  
397 emission estimates for our study region and period than our expected values (figure 5).  
398 Nevertheless, the scale of this discrepancy is underestimated for several reasons. First, we

399 focused solely on necromass carbon losses from understory wildfires whereas GFED and GFAS  
400 include emissions from all land use classes combined. Both databases therefore account for  
401 grassland and agricultural fires, which can affect large areas of human-modified tropical  
402 landscapes. Second, GFED includes both committed and immediate CO<sub>2</sub> emissions. Third, and  
403 again with respect to GFED, fuel loads are much high than those present in our post-  
404 disturbance plots, because they are primarily derived from slash-and-burn and deforestation  
405 studies.

#### 406 (e) Conclusions

407 We demonstrate that there was a substantial loss of necromass following El Niño-mediated  
408 wildfires in the central-eastern Amazon. We conservatively estimate that wildfires in this region  
409 burned 982,276 ha (15.2% of our study region) of primary and secondary forest, resulting in  
410 expected immediate CO<sub>2</sub> emissions of approximately 30 Tg. Better understanding this large and  
411 poorly quantified source of atmospheric carbon is crucial for climate change mitigation efforts.

#### 412 Acknowledgements

413 We thank the four anonymous reviewers for valuable suggestions that improved an earlier  
414 version of the manuscript. We are grateful to the following for financial support: Instituto  
415 Nacional de Ciência e Tecnologia – Biodiversidade e Uso da Terra na Amazônia (CNPq  
416 574008/2008-0), Empresa Brasileira de Pesquisa Agropecuária – Embrapa (SEG:  
417 02.08.06.005.00), the UK government Darwin Initiative (17-023), The Nature Conservancy, and  
418 the UK Natural Environment Research Council (NERC; NE/F01614X/1, NE/G000816/1,  
419 NE/K016431/1, and NE/P004512/1). EB and JB were also funded by H2020-MSCA-RISE-2015  
420 (Project 691053-ODYSSEA). FF is funded by the Brazilian Research Council (CNPq, PELD-  
421 RAS 441659/2016-0). LEOCA thanks the Brazilian Research Council (CNPQ - grants  
422 458022/2013-6 and 305054/2016-3). We thank the Large Scale Biosphere-Atmosphere  
423 Program (LBA) for logistical and infrastructure support during field measurements. We are  
424 deeply grateful to our field and laboratory assistants: Gilson Oliveira, Josué Oliveira, Renílson  
425 Freitas, Marcos Oliveira, Elivan Santos, and Josiane Oliveira. We also thank all collaborating  
426 private landowners for their support and access to their land. This paper is number 69 in the  
427 Rede Amazônia Sustentável publication series.

#### 428 Author contributions

429 JB, FE-S and EB designed the study. EB and JF were responsible for plot selection and  
430 subsequent authorizations from landowners. EB, JB, JF, LEOCA and YM designed the field  
431 protocols. EB, AP, FF, LCR, and KW performed data collection. KW, GDL, AP, EB and CVJS  
432 performed data analyses. KW, GDL, EB, and JB wrote the paper with input from all co-authors.

#### 433 Data accessibility

434 The field data and code used in this paper have been deposited at  
435 <https://doi.org/10.6084/m9.figshare.7059494>. The satellite imagery is available from USGS  
436 (see <https://landsat.usgs.gov/landsat-data-access>). The GFED and GFAS dataset are available

437 from <https://www.globalfiredata.org/data.html> and <http://apps.ecmwf.int/datasets/data/cams->  
438 [gfas/](https://www.globalfiredata.org/data.html), respectively.

## 439 References

- 440 1. Wang W *et al.* 2013 Variations in atmospheric CO<sub>2</sub> growth rates coupled with tropical  
441 temperature. *Proc. Natl. Acad. Sci. U. S. A.* **110**, 13061–6.  
442 (doi:10.1073/pnas.1219683110)
- 443 2. Betts RA, Jones CD, Knight JR, Keeling RF, Kennedy JJ. 2016 El Niño and a record CO<sub>2</sub>  
444 rise. *Nat. Clim. Chang.* **6**, 806–810. (doi:10.1038/nclimate3063)
- 445 3. Zeng N, Qian H, Roedenbeck C, Heimann M. 2005 Impact of 1998-2002 midlatitude  
446 drought and warming on terrestrial ecosystem and the global carbon cycle. *Geophys.*  
447 *Res. Lett.* **32**, n/a-n/a. (doi:10.1029/2005GL024607)
- 448 4. Wang J, Zeng N, Wang M, Jiang F, Wang H, Jiang Z. 2018 Contrasting terrestrial carbon  
449 cycle responses to the 1997/98 and 2015/16 extreme El Niño events. *Earth Syst. Dynam*  
450 **95194**, 1–14. (doi:10.5194/esd-9-1-2018)
- 451 5. Fanin T, Van Der Werf GR. 2015 Relationships between burned area, forest cover loss,  
452 and land cover change in the Brazilian Amazon based on satellite data. *Biogeosciences*  
453 **12**, 6033–6043. (doi:10.5194/bg-12-6033-2015)
- 454 6. Andela N *et al.* 2017 A human-driven decline in global burned area. *Science* **356**, 1356–  
455 1362. (doi:10.1126/science.aal4108)
- 456 7. Arora VK, Melton JR. 2018 Reduction in global area burned and wildfire emissions since  
457 1930s enhances carbon uptake by land. *Nat. Commun.* **9**, 1326. (doi:10.1038/s41467-  
458 018-03838-0)
- 459 8. Hardesty J, Myers R, Fulks W. 2005 Fire, Ecosystems, and People: A Preliminary  
460 Assessment of Fire as a Global Conservation Issue. *George Wright Forum.* **22**, 78–87.  
461 (doi:10.2307/43597968)
- 462 9. Aragão LEOC, Shimabukuro YE. 2010 The incidence of fire in Amazonian forests with  
463 implications for REDD. *Science* **328**, 1275–8. (doi:10.1126/science.1186925)
- 464 10. Aragão LEOC *et al.* 2018 21st Century drought-related fires counteract the decline of  
465 Amazon deforestation carbon emissions. *Nat. Commun.* **9**, 536. (doi:10.1038/s41467-  
466 017-02771-y)
- 467 11. van Marle MJE, Field RD, van der Werf GR, Estrada de Wagt IA, Houghton RA, Rizzo L  
468 V., Artaxo P, Tsigaridis K. 2017 Fire and deforestation dynamics in Amazonia (1973-  
469 2014). *Global Biogeochem. Cycles* **31**, 24–38. (doi:10.1002/2016GB005445)
- 470 12. Jolly WM, Cochrane MA, Freeborn PH, Holden ZA, Brown TJ, Williamson GJ, Bowman  
471 DMJS. 2015 Climate-induced variations in global wildfire danger from 1979 to 2013. *Nat.*  
472 *Commun.* **6**, 7537. (doi:10.1038/ncomms8537)
- 473 13. Pivello VR. 2011 The Use of Fire in the Cerrado and Amazonian Rainforests of Brazil:  
474 Past and Present. *Fire Ecol.* **7**, 24–39. (doi:10.4996/fireecology.0701024)

- 475 14. Chen Y, Randerson JT, Morton DC, DeFries RS, Collatz GJ, Kasibhatla PS, Giglio L, Jin  
476 Y, Marlier ME. 2011 Forecasting Fire Season Severity in South America Using Sea  
477 Surface Temperature Anomalies. *Science (80-. )*. **334**, 787–791.
- 478 15. Brando PM *et al.* 2014 Abrupt increases in Amazonian tree mortality due to drought-fire  
479 interactions. *Proc. Natl. Acad. Sci. U. S. A.* **111**, 6347–52.  
480 (doi:10.1073/pnas.1305499111)
- 481 16. Barlow J, Peres CA, Lagan BO, Hugaasen T. 2003 Large tree mortality and the decline  
482 of forest biomass following Amazonian wildfires. *Ecol. Lett.* **6**, 6–8. (doi:10.1046/j.1461-  
483 0248.2003.00394.x)
- 484 17. Barlow J, Peres CA. 2004 Ecological responses to el Niño-induced surface fires in central  
485 Brazilian Amazonia: management implications for flammable tropical forests. *Philos.*  
486 *Trans. R. Soc. Lond. B. Biol. Sci.* **359**, 367–80. (doi:10.1098/rstb.2003.1423)
- 487 18. Brando PM, Oliveria-Santos C, Rocha W, Cury R, Coe MT. 2016 Effects of experimental  
488 fuel additions on fire intensity and severity: unexpected carbon resilience of a neotropical  
489 forest. *Glob. Chang. Biol.* **22**, 2516–2525. (doi:10.1111/gcb.13172)
- 490 19. Cochrane MA, Schulze MD. 1999 Fire as a Recurrent Event in Tropical Forests of the  
491 Eastern Amazon: Effects on Forest Structure, Biomass, and Species Composition1.  
492 *Biotropica* **31**, 2–16. (doi:10.1111/j.1744-7429.1999.tb00112.x)
- 493 20. Alencar A, Asner GP, Knapp D, Zarin D. 2011 Temporal variability of forest fires in  
494 eastern Amazonia. *Ecol. Appl.* **21**, 2397–2412. (doi:10.1890/10-1168.1)
- 495 21. Cochrane MA, Alencar A, Schulze MD, Souza CM, Nepstad DC, Lefebvre P, Davidson  
496 EA. 1999 Positive feedbacks in the fire dynamic of closed canopy tropical forests.  
497 *Science* **284**, 1832–5. (doi:10.1126/SCIENCE.284.5421.1832)
- 498 22. CVJ S, et al. In press. Drought-induced Amazonian wildfires instigate a decadal-scale  
499 disruption of forest carbon dynamics. *Phil. Trans. R. Soc. B*  
500 (doi:doi:10.1098/rstb.2018.0043)
- 501 23. van der Laan-Luijkx IT *et al.* 2015 Response of the Amazon carbon balance to the 2010  
502 drought derived with CarbonTracker South America. *Global Biogeochem. Cycles* **29**,  
503 1092–1108. (doi:10.1002/2014GB005082)
- 504 24. Liu J *et al.* 2017 Contrasting carbon cycle responses of the tropical continents to the  
505 2015–2016 El Niño. *Science (80-. )*. **358**. (doi:10.1126/science.aam5690)
- 506 25. Gatti L V. *et al.* 2014 Drought sensitivity of Amazonian carbon balance revealed by  
507 atmospheric measurements. *Nature* **506**, 76–80. (doi:10.1038/nature12957)
- 508 26. Pan Y *et al.* 2011 A large and persistent carbon sink in the world's forests. *Science* **333**,  
509 988–93. (doi:10.1126/science.1201609)
- 510 27. Chao K-J, Phillips OL, Baker TR, Peacock J, Lopez-Gonzalez G, Vásquez Martínez R,  
511 Monteagudo A, Torres-Lezama A. 2009 After trees die: quantities and determinants of  
512 necromass across Amazonia. *Biogeosciences* **6**, 1615–1626. (doi:10.5194/bg-6-1615-  
513 2009)
- 514 28. Palace M, Keller M, Hurtt G, Frohling S. 2012 A Review of Above Ground Necromass in

- 515 Tropical Forests. In *Tropical Forests*, InTech. (doi:10.5772/33085)
- 516 29. Ray D, Nepstad D, Moutinho P. 2005 MICROMETEOROLOGICAL AND CANOPY  
517 CONTROLS OF FIRE SUSCEPTIBILITY IN A FORESTED AMAZON LANDSCAPE.  
518 *Ecol. Appl.* **15**, 1664–1678. (doi:10.1890/05-0404)
- 519 30. Keller M, Palace M, Asner GP, Pereira R, Silva JNM. 2004 Coarse woody debris in  
520 undisturbed and logged forests in the eastern Brazilian Amazon. *Glob. Chang. Biol.* **10**,  
521 784–795. (doi:10.1111/j.1529-8817.2003.00770.x)
- 522 31. Palace M, Keller M, Asner GP, Silva JNM, Passos C. 2007 Necromass in undisturbed  
523 and logged forests in the Brazilian Amazon. *For. Ecol. Manage.* **238**, 309–318.  
524 (doi:10.1016/J.FORECO.2006.10.026)
- 525 32. Keenan RJ, Reams GA, Achard F, de Freitas J V., Grainger A, Lindquist E. 2015  
526 Dynamics of global forest area: Results from the FAO Global Forest Resources  
527 Assessment 2015. *For. Ecol. Manage.* **352**, 9–20. (doi:10.1016/J.FORECO.2015.06.014)
- 528 33. Cochrane MA. 2003 Fire science for rainforests. *Nature* **421**, 913–919.  
529 (doi:10.1038/nature01437)
- 530 34. Uhl C, Kauffman JB. 1990 Deforestation, Fire Susceptibility, and Potential Tree  
531 Responses to Fire in the Eastern Amazon. *Ecology* **71**, 437–449. (doi:10.2307/1940299)
- 532 35. Alencar A, Nepstad D, Del Carmen Vera Diaz M. 2006 Forest understory fire in the  
533 Brazilian Amazon in ENSO and non-ENSO years: Area burned and committed carbon  
534 emissions. *Earth Interact.* **10**. (doi:10.1175/EI150.1)
- 535 36. Van Leeuwen TT *et al.* 2014 Biomass burning fuel consumption rates: A field  
536 measurement database. *Biogeosciences* **11**, 7305–7329. (doi:10.5194/bg-11-7305-2014)
- 537 37. Berenguer E *et al.* 2014 A large-scale field assessment of carbon stocks in human-  
538 modified tropical forests. *Glob. Chang. Biol.* **20**, 3713–3726. (doi:10.1111/gcb.12627)
- 539 38. Gardner TA *et al.* 2013 A social and ecological assessment of tropical land uses at  
540 multiple scales: the Sustainable Amazon Network. *Philos. Trans. R. Soc. Lond. B. Biol.*  
541 *Sci.* **368**, 20120166. (doi:10.1098/rstb.2012.0166)
- 542 39. Hughes RF, Kauffman JB, Jaramillo VJ. 1999 Biomass, carbon, and nutrient dynamics of  
543 secondary forests in a humid tropical region of México. *Ecology* **80**, 1892–1907.  
544 (doi:10.1890/0012-9658(1999)080[1892:BCANDO]2.0.CO;2)
- 545 40. Cummings DL, Boone Kauffman J, Perry DA, Flint Hughes R. 2002 Aboveground  
546 biomass and structure of rainforests in the southwestern Brazilian Amazon. *For. Ecol.*  
547 *Manage.* **163**, 293–307. (doi:10.1016/S0378-1127(01)00587-4)
- 548 41. Keller M, Palace M, Asner GP, Pereira R, Silva JNM. 2004 Coarse woody debris in  
549 undisturbed and logged forests in the eastern Brazilian Amazon. *Glob. Chang. Biol.* **10**,  
550 784–795. (doi:10.1111/j.1529-8817.2003.00770.x)
- 551 42. Eggleston HS, Intergovernmental Panel on Climate Change. National Greenhouse Gas  
552 Inventories Programme S ed., Chikyū Kankyō Senryaku Kenkyū Kikan L ed., Miwa K.  
553 2006 *2006 IPCC guidelines for national greenhouse gas inventories*. Kanagawa, JP :  
554 Institute for Global Environmental Strategies. See <http://www.sidalc.net/cgi->

- 555 bin/wxis.exe/?IsisScript=earth.xis&method=post&formato=2&cantidad=1&expresion=mfn  
556 =001720.
- 557 43. Marthews TR. In press. Measuring Tropical Forest Carbon Allocation and Cycling v3.0 A  
558 RAINFOR-GEM Field Manual for Intensive Census Plots.
- 559 44. Akagi SK, Yokelson RJ, Wiedinmyer C, Alvarado MJ, Reid JS, Karl T, Crouse JD,  
560 Wennberg PO. 2011 Emission factors for open and domestic biomass burning for use in  
561 atmospheric models. *Atmos. Chem. Phys.* **11**, 4039–4072. (doi:10.5194/acp-11-4039-  
562 2011)
- 563 45. van der Werf GR *et al.* 2017 Global fire emissions estimates during 1997–2016. *Earth*  
564 *Syst. Sci. Data* **9**, 697–720. (doi:10.5194/essd-9-697-2017)
- 565 46. Kaiser JW *et al.* 2012 Biomass burning emissions estimated with a global fire assimilation  
566 system based on observed fire radiative power. *Biogeosciences* **9**, 527–554.  
567 (doi:10.5194/bg-9-527-2012)
- 568 47. Bank W. 2018 CO2 emissions. See  
569 <https://data.worldbank.org/indicator/EN.ATM.CO2E.KT?view=chart> (accessed on 27 April  
570 2018).
- 571 48. Bustamante MMC *et al.* 2016 Toward an integrated monitoring framework to assess the  
572 effects of tropical forest degradation and recovery on carbon stocks and biodiversity.  
573 *Glob. Chang. Biol.* **22**, 92–109. (doi:10.1111/gcb.13087)
- 574 49. Barlow J *et al.* 2012 The critical importance of considering fire in REDD+ programs. *Biol.*  
575 *Conserv.* **154**, 1–8. (doi:10.1016/J.BIOCON.2012.03.034)
- 576 50. Dai A. 2013 Increasing drought under global warming in observations and models. *Nat.*  
577 *Clim. Chang.* **3**, 52–58. (doi:10.1038/nclimate1633)
- 578 51. Malhi Y, Roberts JT, Betts RA, Killeen TJ, Li W, Nobre CA. 2008 Climate Change,  
579 Deforestation, and the Fate of the Amazon. **169**. (doi:10.1126/science.1146961)
- 580 52. Spracklen D V., Garcia-Carreras L. 2015 The impact of Amazonian deforestation on  
581 Amazon basin rainfall. *Geophys. Res. Lett.* **42**, 9546–9552. (doi:10.1002/2015GL066063)
- 582 53. Soares-Filho B *et al.* 2010 Role of Brazilian Amazon protected areas in climate change  
583 mitigation. *Proc. Natl. Acad. Sci. U. S. A.* **107**, 10821–6. (doi:10.1073/pnas.0913048107)
- 584 54. Palace M, Keller M, Asner GP, Silva JNM, Passos C. 2007 Necromass in undisturbed  
585 and logged forests in the Brazilian Amazon. *For. Ecol. Manage.* **238**, 309–318.  
586 (doi:10.1016/j.foreco.2006.10.026)
- 587 55. Chambers JQ, Higuchi N, Schimel JP, Ferreira L V., Melack JM. 2000 Decomposition and  
588 carbon cycling of dead trees in tropical forests of the central Amazon. *Oecologia* **122**,  
589 380–388. (doi:10.1007/s004420050044)
- 590 56. Berenguer E, Gardner TA, Ferreira J, Aragão LEOC, Mac Nally R, Thomson JR, Vieira  
591 ICG, Barlow J. 2018 Seeing the woods through the saplings: Using wood density to  
592 assess the recovery of human-modified Amazonian forests. *J. Ecol.* (doi:10.1111/1365-  
593 2745.12991)

594 57. Durigan MR *et al.* 2017 Soil Organic Matter Responses to Anthropogenic Forest  
595 Disturbance and Land Use Change in the Eastern Brazilian Amazon. *Sustainability* 9,  
596 379. (doi:10.3390/su9030379)

597

## 598 Figure legends

599 Figure 1. (a) The 2017 land-use map across the ~6.5 million ha study region. (b) The land-use  
600 map within the RAS study area (shown by the white border in (a)). Also shown in this panel are  
601 the locations of the 107 study plots (black circles). The 18 of these that were used for  
602 necromass monitoring are shown as orange circles. The inset shows the Santarém study region  
603 (red circle) within South America, the Brazilian Amazon (green), and Pará (white border).

604 Figure 2. Necromass carbon stocks in leaf litter (a), fine woody debris (FWD; b), coarse woody  
605 debris (CWD; c), dead standing stems (d), and the total across all components (e) in human-  
606 modified Amazonian forests. Boxplots show the interquartile range. Letters above the boxplots  
607 show the results from multiple pairwise comparisons of forest class medians. Classes that do  
608 not share a letter have significantly different medians ( $p < 0.05$ ).

609 Figure 3. The relationship between percentage reduction in necromass carbon stocks and fire  
610 intensity (a), as measured by median char height, and plot-level estimates of burned area (b) in  
611 human-modified Amazonian forests.

612 Figure 4. Pre- vs post-El Niño necromass carbon stocks in unburned control sites (a) and sites  
613 burned in 2015-16 (b), and pre-El Niño necromass carbon stocks vs post-El Niño necromass  
614 losses in unburned control sites (c) and sites burned in 2015-16 (d) in human-modified  
615 Amazonian forests. In panel (a) the black line shows the significant ( $p < 0.001$ ) relationship  
616 between pre- and post-El Niño necromass carbon stocks in unburned sites. The equation for  
617 this relationship is shown in the panel. The grey band represents 1 s.e.m. Note that, due to data  
618 limitations, pre- and post-El Niño necromass totals are based on coarse and fine woody debris  
619 and leaf litter only (i.e. dead standing stems are not included).

620 Figure 5. CO<sub>2</sub> emissions for wildfires in central-eastern Amazonian human-modified tropical  
621 forests. Points show expected emissions for four land-use scenarios (see Section 2e and table  
622 S1): a, prim1 + sec1; b, prim2 + sec1; c, prim1 + sec2; d, prim2 + sec2. Error bars show CO<sub>2</sub>  
623 emission 95% confidence intervals. Also shown are cumulative CO<sub>2</sub> emissions for our study  
624 region and period from the Global Fire Emissions Database (dotted line) and the Global Fire  
625 Assimilation System (dashed line).

626 Figure 6: Comparing our findings to those from the Global Fire Assimilation System (GFAS) and  
627 the Global Fire Emissions Database (GFED). CO<sub>2</sub> emissions for our study region and period  
628 from GFAS (a) and our emissions shown at the same scale (0.1 degrees; (b)). CO<sub>2</sub> emissions  
629 from GFED (c) and our emissions shown at the same scale (0.25 degrees; (d)). The proportion  
630 of land burned for our study region and period from GFED (e) and our estimate of burned area  
631 shown at the same scale (0.25 degrees; (f)). In all panels, our Landsat-derived fire map is  
632 shown in dark green, deforestation in light grey, and water in blue.

633 Table 1: Forest classifications for pre-El Niño forest disturbance classes and the plot samples in  
 634 2010, 2014-15 and 2017. The 2015-16 sample occurred after the extensive wildfires and is a  
 635 subset of the 2014-15 sample.

<b>Pre-El Niño forest class</b>	<b>Definition</b>	<b>Necromass assessment (2010)</b>	<b>Monitoring of coarse woody debris (2014-2015)</b>	<b>Burned in 2015-16 and sampled in 2017</b>	<b>Fire intensity and plot burned area (2017)</b>
<b>Undisturbed primary forest</b>	Primary forest with no evidence of human disturbance, such as fire scars or standing tree damage	17	5	2	3
<b>Logged primary forest</b>	Primary forest with evidence of logging, such as logging debris	26	5	4	1
<b>Burned primary forest</b>	Primary forest with evidence of recent fire, such as fire scars	7	0	0	0
<b>Logged-and-burned primary forest</b>	Primary forest with evidence of both logging and fire	24	4	1	4
<b>Secondary forest</b>	Forest regenerating after complete removal of native vegetation	33	4	0	1

636

637

638

639

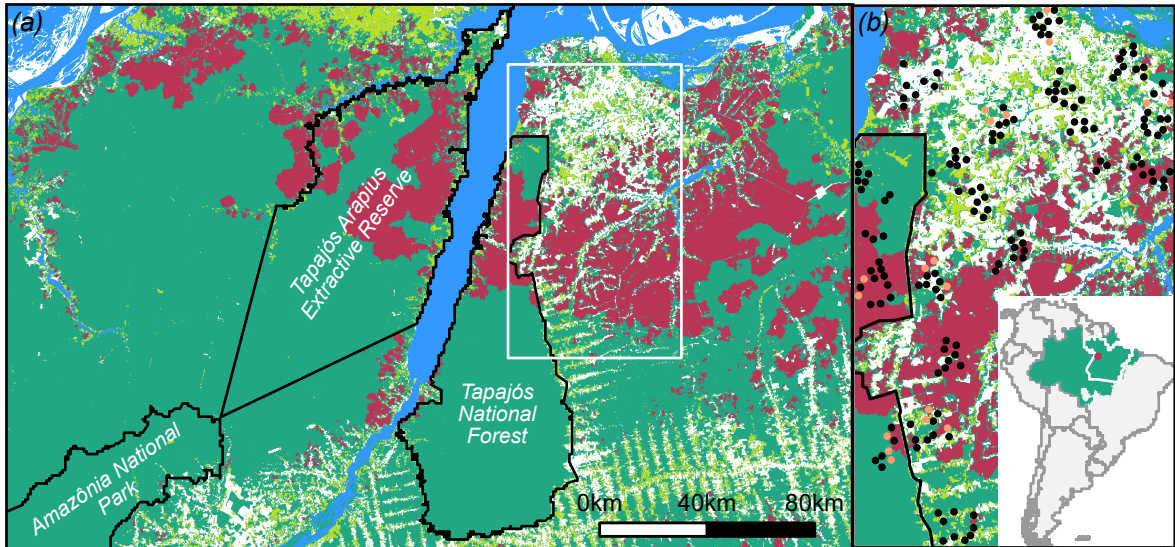
Primary forest

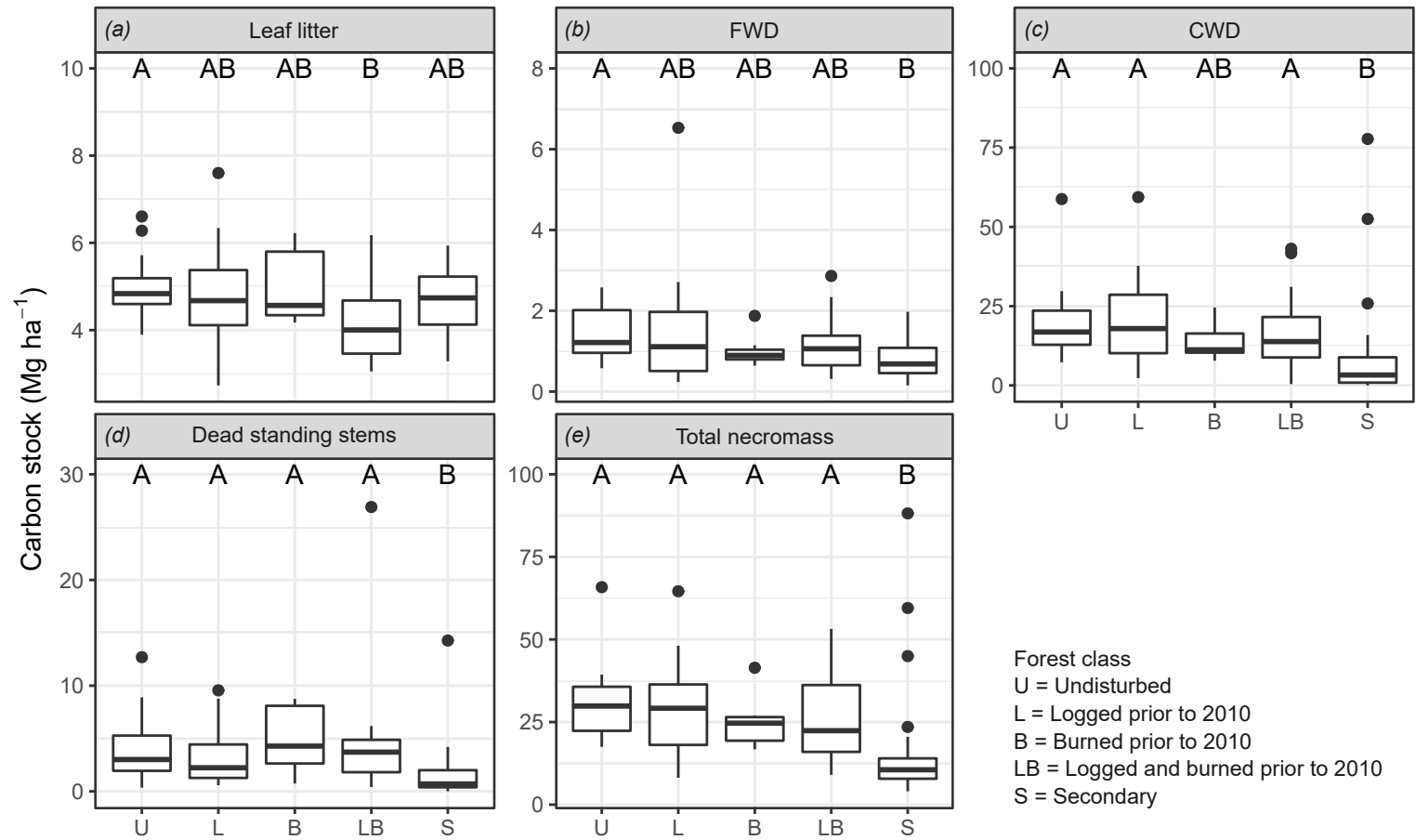
Secondary forest

Burned 2015-16

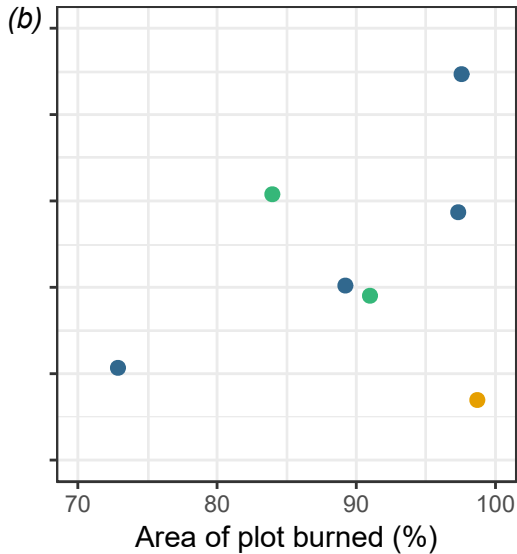
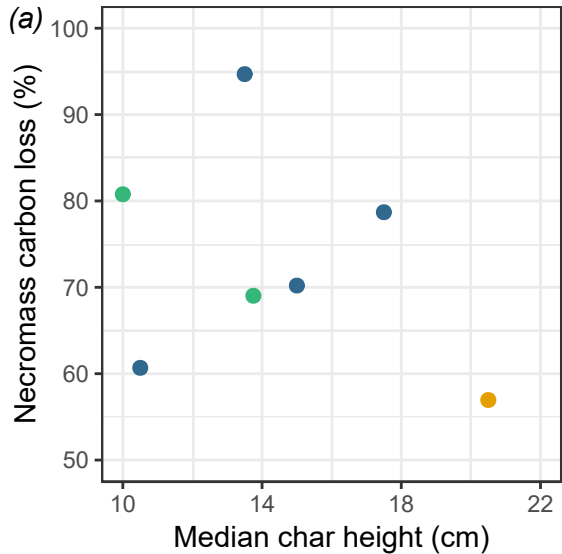
Water

Necromass monitoring

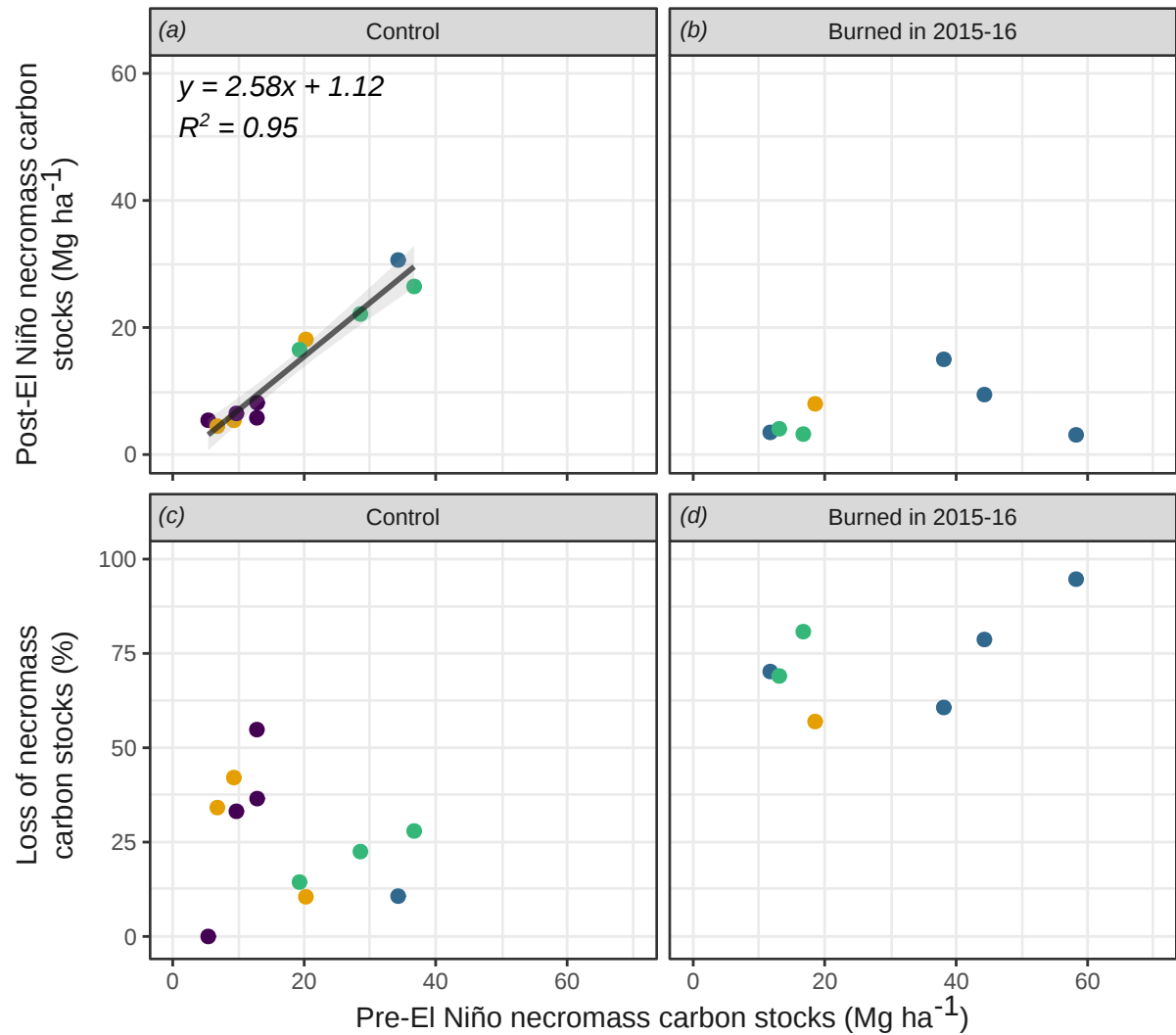


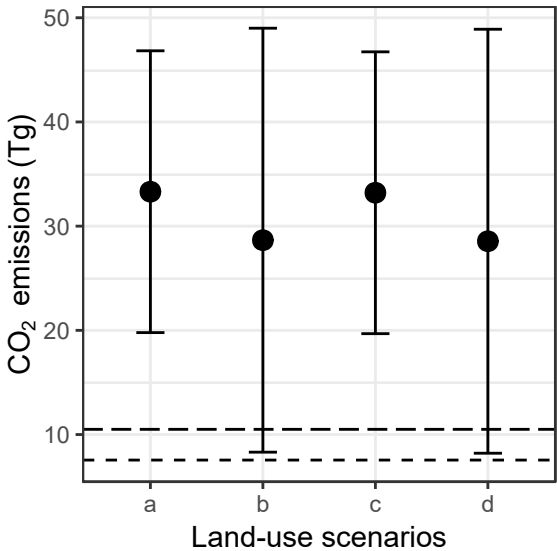


● Undisturbed ● Logged prior to 2010 ● Logged and burned prior to 2010



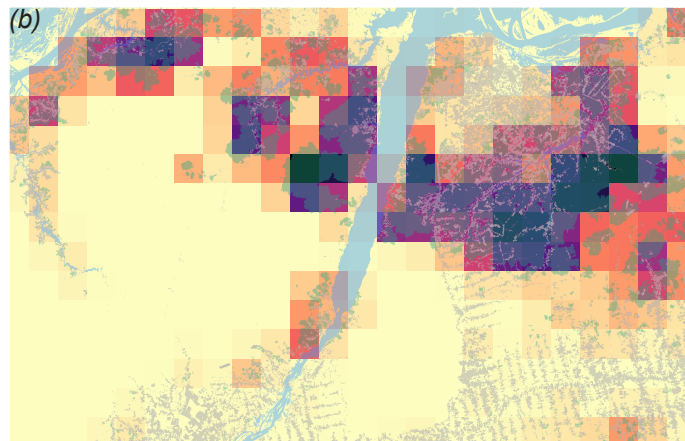
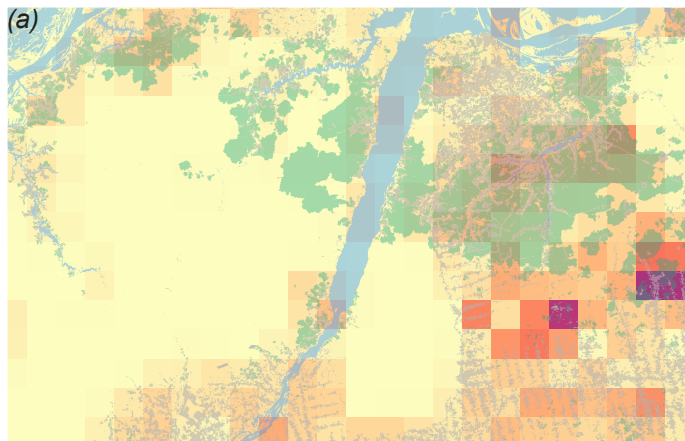
● Undisturbed ● Logged prior to 2010 ● Logged and burned prior to 2010 ● Secondary





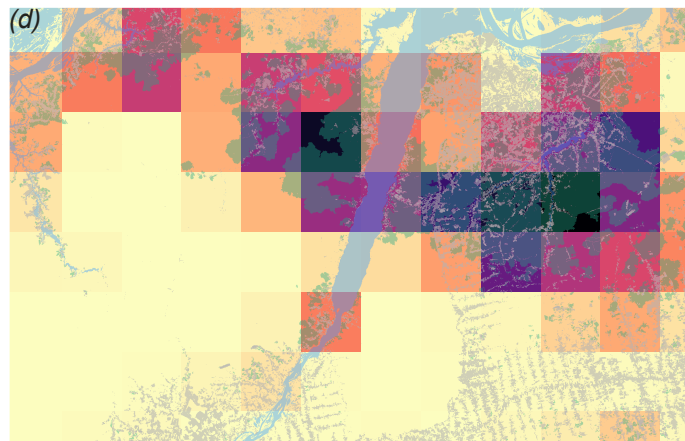
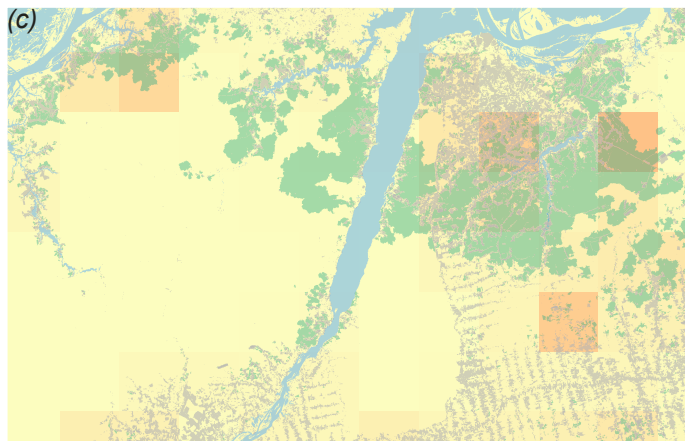
CO<sub>2</sub> emissions (Tg)

0.00 0.29 0.58



CO<sub>2</sub> emissions (Tg)

0.00 0.91 1.82



Proportion burned

0.00 0.37 0.74

